



A general framework for predicting mean profiles in compressible turbulent boundary layers with established scaling laws

Anjia Ying b, Zhigang Li b and Lin Fu 200

Corresponding author: Lin Fu, linfu@ust.hk

(Received 16 June 2025; revised 27 July 2025; accepted 8 September 2025)

A prediction framework for the mean quantities in a compressible turbulent boundary layer (TBL) with given Reynolds number, free-stream Mach number and wall-to-recovery ratio as inputs is proposed based on the established scaling laws regarding the velocity transformations, skin-friction coefficient and temperature-velocity (TV) relations. The established velocity transformations that perform well for collapsing the compressible mean profiles onto incompressible ones in the inner layer are used for the scaling of such inner-layer components of mean velocity, while the wake velocity scaling is determined such that self-consistency is achieved under the scaling law for the skin-friction coefficient. A total of 44 compressible TBLs from six direct numerical simulations databases are used to validate the proposed framework, with free-stream Mach numbers ranging from 0.5 to 14, friction Reynolds numbers ranging from 100 to 2400, and wall-to-recovery ratios ranging from 0.15 to 1.9. When incorporated with the scaling laws for velocity transformation from Griffin et al. (2021, Proc. Natl Acad. Sci., vol. 118, e2111144118), the skin-friction coefficient from Zhao & Fu (2025, J. Fluid Mech., vol. 1012, R3) and the TV relation from Duan & Martín (2011, J. Fluid Mech., vol. 684, pp. 25–59), the prediction errors in the mean velocity and temperature profiles remain within 4.0 % and 6.0 %, respectively, across all tested cases. Correspondingly, the skin-friction and wallheat-transfer coefficients are also accurately predicted, with root mean square prediction errors of approximately 3 %. When adopting different velocity transformation methods that are valid for inner-layer scaling, the root mean square prediction errors in the mean velocity and temperature profiles remain below 2.3 % and 3.6 %, respectively, which further highlights the universality of the proposed framework.

Key words: boundary layers, compressible boundary layers, turbulence modelling

¹Department of Mechanical and Aerospace Engineering, The Hong Kong University of Science and Technology, Clear Water Bay, Kowloon, Hong Kong

²Department of Mathematics, The Hong Kong University of Science and Technology, Clear Water Bay, Kowloon, Hong Kong

1. Introduction

The high-speed turbulent boundary layer (TBL) is known to significantly affect the surface drag and heat transfer, the accurate prediction of which is thus of great importance for reliable vehicle design and flow control (Bradshaw 1977). Numerous studies conducted are engaged in uncovering physical insights in the TBL, based on which fruitful mathematical models in describing the physical properties are extracted (e.g. van Driest 1951; Spalding & Chi 1964; Huang, Bradshaw & Coakley 1993; Duan, Beekman & Martin 2010; Chen, Gan & Fu 2024). As an idealised simplification of the compressible TBL, the incompressible counterpart exhibits distinct universal laws in the mean quantities, such as those for the mean velocity profile in the wall-normal direction (Johnson & King 1985; Kawai & Larsson 2012). However, due to the variations of mean properties such as density and viscosity in the wall-normal direction, the prediction of the mean properties of compressible TBLs with non-negligible Mach numbers is still a challenging task and needs further refinement.

Inspired by Morkovin (1962), where it is hypothesised that the compressible wallbounded flows can be mapped onto incompressible counterparts by accounting for the variations in mean properties, the established scaling laws for incompressible TBLs can be applied in compressible ones with appropriate transformations. Over decades, studies on velocity transformations have been actively conducted (e.g. van Driest 1951; Zhang et al. 2012; Trettel & Larsson 2016; Volpiani et al. 2020; Griffin, Fu & Moin 2021b; Hasan et al. 2023). The pioneer work by van Driest (1951) (denoted as vD) built upon the mixing length assumption performs well in high-speed adiabatic flows but deteriorates for diabatic conditions. On the other hand, the total-stress-based transformation by Griffin et al. (2021b) (denoted as GFM), which is parameter-free, demonstrates exceptional performance in collapsing the mean streamwise velocity profiles of various flow types, including turbulent channel flows, pipe flows and TBLs even with strong heat transfer, into the incompressible counterparts in the inner layers. In addition to GFM, the transformations proposed by Volpiani et al. (2020) (termed Volpiani), which is datadriven, and Hasan et al. (2023) (termed HLPP), by interpreting intrinsic compressibility effects, also perform well in the inner layers of compressible TBLs.

Besides the velocity transformation, the scaling of the skin-friction coefficient in compressible TBLs is a related but different topic. Accounting for the variations in density and viscosity, van Driest (1951) proposes a scaling law for the skin-friction coefficient that is applicable in both compressible and incompressible TBLs. Spalding & Chi (1964) further improve the theory of van Driest (1951) by including the impacts of free-stream Mach number and temperature. However, neither of these two theories provides accurate predictions on the skin-friction coefficient with a very cold wall (Bradshaw 1977). Recently, Zhao & Fu (2025) developed a general scaling law for the skin-friction coefficient based on physical and asymptotic analyses, which precisely predicts the transformed skin-friction coefficient with wide ranges of free-stream Mach numbers and wall-to-recovery ratios. The above-mentioned established scaling laws for velocity transformation and skin-friction coefficient, in combination with the well-established temperature–velocity (TV) relations (e.g. Duan & Martín 2011; Zhang et al. 2014), provide abundant theoretical foundations for modelling the mean quantities of compressible TBLs in the current study.

To predict the mean profiles in compressible TBLs, Huang *et al.* (1993) apply inverse vD transformation to a modelled incompressible velocity profile. Griffin *et al.* (2021*a*) compute the velocity and temperature profiles of compressible wall-bounded turbulence with inverse GFM transformation and TV relation (Zhang *et al.* 2014). Such a strategy is further developed for evaluating the mean profiles, wall shear stress and wall heat

flux for wall-modelled large-eddy simulations (Griffin, Fu & Moin 2023). Kumar & Larsson (2022) also evaluate the entire profile within the boundary layer based on the inverse Volpiani transformation. Despite these advancements, given that the current velocity transformations (e.g. vD, GFM, HLPP and Volpiani) are developed based on the physical properties in the inner layer, the determination of the entire velocity profile depending solely on one scaling law is somehow questionable. To address this, Hasan et al. (2024) separately model the inner and wake components with inverse HLPP and vD transformations, where the scaling factor for the wake component is modelled based on data fitting. However, the scaling factor expressed as a function of the momentumthickness-based Reynolds number Re_{θ} still results in non-negligible data scatter, indicating potential error sources in the predicted results. On the other hand, Chen et al. (2024) propose to predict the mean profiles in the inner and outer layers with inverse GFM and vD transformations, respectively, and splice them at a certain matching point between the two layers. While these approaches show promise, a more reliable framework is needed for appropriate scalings of the entire mean profiles, especially for that in the outer layer.

In our current study, a universal framework for predicting mean profiles of compressible TBLs is proposed based on established scaling laws regarding the velocity transformation, skin-friction coefficient and TV relation, by which the inner and wake components of the mean profiles are properly scaled. No additional data fitting operations are introduced in this framework, allowing it to be feasible to incorporate any velocity transformations with validity in the inner layer. The prediction framework is derived in § 2, with prediction results for the mean quantities presented in § 3. Concluding remarks are provided in § 4.

2. Methodology

The mean-profile-prediction framework to be derived includes the incompressible model for mean velocity, velocity transformation, general scaling law for skin-friction coefficient and TV relation, as elaborated in §§ 2.1, 2.2, 2.3 and 2.4, respectively. They are leveraged to iteratively compute the mean velocity and temperature profiles until the results converge, as summarised in § 2.5.

2.1. Modelling the mean profiles of the incompressible TBL

The mean velocity profile for the incompressible TBL can be expressed by (Coles 1956)

$$U^{inc}(y) = U^{inc}_{inner}\left(\frac{y}{\delta_{\nu}}\right) + \Pi U^{inc}_{wake}\left(\frac{y}{\delta_{e}}\right), \tag{2.1}$$

where y is the wall-normal distance, δ_e is the boundary layer thickness where the mean streamwise velocity is 99 % of the free-stream velocity, $\delta_{\nu} = \nu/u_{\tau}$ is the viscous length, ν is the molecular kinetic viscosity, $u_{\tau} = \sqrt{\tau_w/\rho_w}$ is the friction velocity, $\tau_w = (\rho \partial_y U)_w$ is the wall shear stress, ρ is the mean density and the subscript w denotes the quantities at the wall. In this study, the velocities and lengths with superscripts + denote those normalised by u_{τ} and δ_{ν} . For instance, $U^{inc,+} = U^{inc}/u_{\tau}$ and $y^+ = y/\delta_{\nu}$. Assuming equilibrium, the inner component of the mean velocity profile can be expressed with (Kawai & Larsson 2012)

$$\frac{\mathrm{d}U_{inner}^{inc}(y/\delta_{\nu})}{\mathrm{d}y} = \frac{u_{\tau}}{\delta_{\nu}} \frac{1}{1 + \mu_{t}/\mu},\tag{2.2}$$

where $\mu = \rho \nu$ is the molecular dynamic viscosity, and μ_t is the eddy dynamic viscosity. The Johnson-King model (Johnson & King 1985) that is built upon the arguments of

the mixing length model (van Driest 1956) is adopted to describe the eddy dynamic viscosity, i.e.

$$\mu_t = \kappa \rho y \sqrt{\frac{\tau_w}{\rho}} \mathcal{D}, \quad \mathcal{D} = \left[1 - \exp\left(-y^+/A^+\right)\right]^2,$$
 (2.3)

with $\kappa = 0.41$ and $A^+ = 17$. On the other hand, Coles' wake function (Coles 1956) is adopted to describe $U^{inc}_{wake}(y/\delta_e)$, which is the normalised shape of the wake component of the mean velocity profile, as expressed by

$$\frac{\mathrm{d}U_{wake}^{inc}(y/\delta_e)}{\mathrm{d}y} = \frac{u_\tau}{\delta_e} \frac{\pi}{\kappa} \sin\left(\pi \frac{y}{\delta_e}\right). \tag{2.4}$$

According to Coles' law of the wake (Coles 1956), the wake scaling factor Π for a zero-pressure-gradient incompressible TBL can be approximately treated as a constant 0.55. In our proposed framework, Coles' law of the wake is further extended to the compressible TBL by determining Π based on the self-consistency criterion regarding the general scaling law for C_f (Zhao & Fu 2025), as illustrated in the next subsection.

The inner component U_{inner}^{inc} in (2.2) and normalised wake component U_{wake}^{inc} in (2.4) of the incompressible TBL introduced in this subsection will be utilised for constructing the compressible counterparts, as derived in the following.

2.2. Shaping the mean profiles of compressible TBLs with velocity transformations. In this study, the mean streamwise velocity profile of a compressible TBL is reconstructed with

$$U = U_{inner} + \Pi U_{wake}, \tag{2.5}$$

where U_{inner} and U_{wake} are inversely transformed from U_{inner}^{inc} and U_{wake}^{inc} , respectively. Given the validity of the established velocity transformations (e.g. GFM, HLPP and Volpiani) in the inner layer, U_{inner}^{inc} can be readily transformed to the compressible counterpart with these methods. With inverse GFM transformation applied, for example, the mean velocity in an incompressible TBL compared to that in a compressible TBL with the same Re_{τ}^* is expressed by

$$\frac{dU_{inner}^{+}}{dy^{*}} = \frac{\frac{dU_{inner}^{inner}}{dy^{*}}}{\frac{1}{\mu^{+}} - \frac{1}{\mu^{+}} \frac{dU_{inner}^{inc,+}}{dy^{*}} + \mu^{+} \frac{dU_{inner}^{inc,+}}{dy^{+}}},$$
 (2.6)

where $y^* = y/\delta_v^*$, $Re_\tau^* = \delta_e/\delta_v^*(y = \delta_e)$, $\delta_v^*(y) = v(y)/u_\tau^*(y)$ is the semi-local length scale, $u_\tau^*(y) = \sqrt{\tau_w/\rho(y)}$ is the semi-local velocity scale, and $\mu^+ = \mu/\mu_w$. The derivations of the inverse GFM transformation (2.6) are provided in Appendix A. In the rest of this paper, the inverse GFM transformation is the default method for inner scalings unless otherwise stated.

On the other hand, most of the currently available velocity transformations are fundamentally based on the physical characteristics of the inner layer, which results in a less robust foundation for outer scaling when compared to the well-established inner scaling. As a practical compromise without sacrificing generality, the inverse vD transformation that provides fair scaling of U_{wake} (Duan, Beekman & Martin 2011; Chen et al. 2024) is employed for outer scaling in the tests conducted in this study:

$$\frac{\mathrm{d}U_{wake}^{+}}{\mathrm{d}y^{*}} = \sqrt{\frac{1}{\rho^{+}}} \frac{\mathrm{d}U_{wake}^{inc,+}}{\mathrm{d}y^{*}},\tag{2.7}$$

where $\rho^+ = \rho/\rho_w$. Note that the transformation for outer scaling can be replaced with more reliable methods developed in future studies.

2.3. Determining the wake scaling factor with the general scaling law for C_f

To determine the wake scaling factor Π , the general scaling law for C_f recently proposed by Zhao & Fu (2025) is introduced. In their theory, the redefined skin friction coefficient $C_{f,i}$ closely matches the predicted value as a function of the redefined momentum-thickness-based Reynolds number $Re_{\theta,i}$ in actual compressible TBLs within a fairly wide range of flow conditions. The redefined skin-friction coefficient is described with

$$\left(\frac{2}{C_{f,i}}\right)^{1/2} = \frac{1}{\kappa_f} \ln Re_{\theta,i} + C,$$
 (2.8)

with $\kappa_f = 0.344$ and C = 1.770. Here, $C_{f,i}$ and $Re_{\theta,i}$ are defined by

$$C_{f,i} = F_{C^*}C_f, \quad Re_{\theta,i} = F_{\theta^*}Re_{\theta^*}, \tag{2.9}$$

with $F_{C^*} = (\rho_{\infty}/\rho_w)F^{-2}$, $F_{\theta^*} = (\rho_w\mu_{\infty}/(\rho_{\infty}\mu_w))F$ and $F = U_{\infty}^{inc,+}/U_{\infty}^+$. Here, the subscript ∞ denotes the free-stream quantities, and $U^{inc,+}$ is obtained from the forward GFM transformation that is formulated by

$$\frac{\mathrm{d}U^{inc,+}}{\mathrm{d}y^*} = \frac{\frac{1}{\mu^+} \frac{\mathrm{d}U^+}{\mathrm{d}y^*}}{1 + \frac{1}{\mu^+} \frac{\mathrm{d}U^+}{\mathrm{d}y^*} - \mu^+ \frac{\mathrm{d}U^+}{\mathrm{d}y^+}}.$$
 (2.10)

In (2.9), Re_{θ^*} is expressed as $Re_{\theta^*} = U_{\infty}\theta^*/\mu_{\infty}$, with

$$\theta^* = \int_0^{\delta_e} \frac{\rho}{\rho_\infty} \frac{U^{inc,+}}{U_\infty^{inc,+}} \left(1 - \frac{U^{inc,+}}{U_\infty^{inc,+}} \right) d\left(y^* \delta_\nu \right). \tag{2.11}$$

Based on (2.8)–(2.11), the skin-friction coefficient can be predicted with

$$C_f = 2 / \left[F_{C^*} \left(\frac{1}{\kappa_f} \ln Re_{\theta,i} + C \right)^2 \right]. \tag{2.12}$$

Since the above theory accurately describes the skin-friction coefficient for TBLs within a vast range of flow conditions, it provides an important criterion to judge the self-consistency of the predicted results from the to-be-proposed framework. Hence we propose to determine the wake scaling factor Π such that the discrepancy between the predicted C_f directly from definition, i.e. $C_f = \tau_w/(0.5\rho_\infty U_\infty^2) = 2/(\rho_\infty^+ U_\infty^{+2})$, and that from (2.12) is lower than 10^{-5} , which can be derived to be

$$|\epsilon| = \left| \rho_{\infty}^+ U_{\infty}^{+2} \middle/ \left\lceil F_{C^*} \left(\frac{1}{\kappa_f} \ln Re_{\theta,i} + C \right)^2 \right\rceil - 1 \right| \leqslant 10^{-5}. \tag{2.13}$$

An *a priori* test is conducted here by reconstructing the mean velocity profile with actual mean temperature from the direct numerical simulations (DNS) such that the performance of the proposed self-consistency criterion (2.13) in determining the wake scaling factor is scrutinised individually. The prediction error of $U^+(y)$ is investigated in this test, which is defined by

$$\mathcal{E}(U^{+}) = \sqrt{\frac{1}{\delta_{e}} \int_{0}^{\delta_{e}} \left(U_{P}^{+}(\eta) - U_{DNS}^{+}(\eta) \right)^{2} d\eta} / \left(\frac{1}{\delta_{e}} \int_{0}^{\delta_{e}} U_{DNS}^{+}(\eta) d\eta \right), \tag{2.14}$$
1021 A30-5

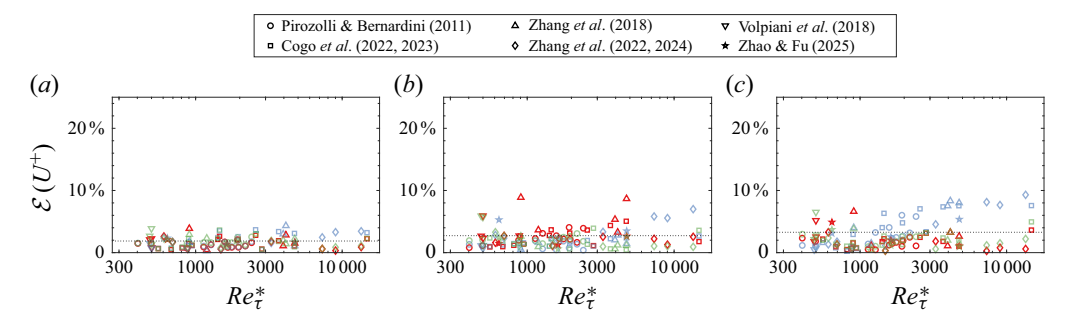


Figure 1. A priori test for prediction errors of the mean velocity profile in the results from (a) present framework, (b) empirical formulation in Hasan et al. (2024), and (c) direct inverse transformation as in Kumar & Larsson (2022) for inner-layer scaling. The black dotted lines denote the root mean square values of the prediction errors for all the considered cases. The red, blue and green symbols denote the results from GFM, HLPP and Volpiani.

where the subscripts P and DNS denote the predicted and DNS results, respectively. The prediction errors based on a total of 44 compressible TBLs from six DNS databases (Pirozzoli & Bernardini 2011; Volpiani, Bernardini & Larsson 2018; Zhang, Duan & Choudhari 2018; Cogo $et\ al.\ 2022,\ 2023;$ Zhang $et\ al.\ 2022,\ 2024;$ Zhao & Fu 2025) are summarised in figure 1. Detailed flow parameters of these 44 test cases are summarised in Appendix B. Note that all of these cases will be further used for comprehensive validations of the to-be-proposed framework in the following parts of this study. For comparison, the results from the empirical formulation of the compressible mean profile in Hasan $et\ al.\ (2024)$ and direct inverse transformation of the incompressible counterparts as proposed by Kumar & Larsson (2022) are also included in figure 1. In all the tested cases, the prediction errors from the presented framework are lower than 5.0 % regardless of the specific choice of the velocity transformation method among GFM, HLPP and Volpiani for inner scaling with root mean square values equal to 1.9 %, which is much lower than those from the other two frameworks. The validity of the self-consistency criterion regarding the general scaling law of C_f in determining the wake scaling factor is thus demonstrated.

To further investigate how the wake scaling factor Π varies with increasing free-stream Mach number M_{∞} , the results of Π determined from the criterion (2.13) with actual mean temperature from DNS are summarised in figure 2. For subsonic flow with $M_{\infty}=0.5$ from Zhang *et al.* (2022), the value of Π is 0.48, which is close to the recommended value 0.55 for incompressible flows (Coles 1956). As M_{∞} increases, Π tends to decrease. In particular, for all hypersonic cases with $M_{\infty} \geqslant 5.0$, Π falls below 0.35. This dependence of the wake scaling factor Π on the free-stream Mach number underscores the importance of accounting for compressibility effects when modelling mean profiles in high-speed wall-bounded turbulent flows.

2.4. Determining mean temperature with TV relation

The mean temperature profile can be evaluated from the established TV relationships. In the following test cases in this study, the TV relation established by Duan & Martín (2011) is adopted to determine the mean temperature profile from the velocity, which is formulated as

$$\frac{T}{T_e} = \frac{T_w}{T_e} + \frac{T_r - T_w}{T_e} \left[(1 - sPr) \left(\frac{U}{U_e} \right)^2 + sPr \left(\frac{U}{U_e} \right) \right] + \frac{T_e - T_r}{T_e} \left(\frac{U}{U_e} \right)^2, \quad (2.15)$$

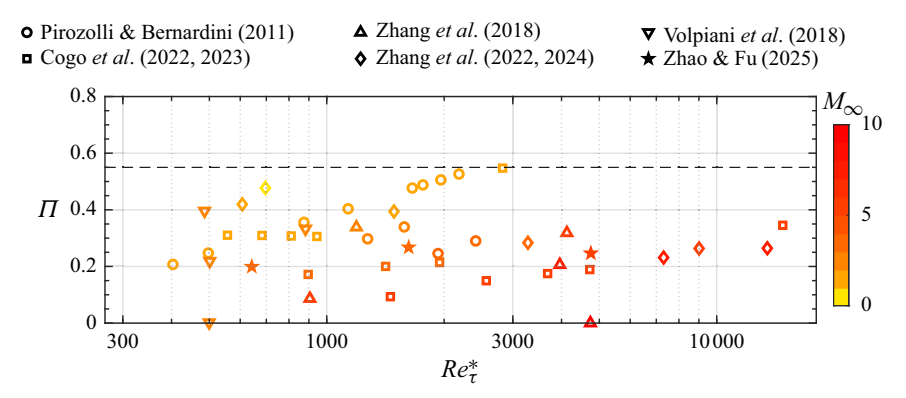


Figure 2. Values of Π for compressible TBLs with GFM for inner-layer scaling. The black dashed line denotes $\Pi = 0.55$ as suggested by Coles (1956) for incompressible TBLs.

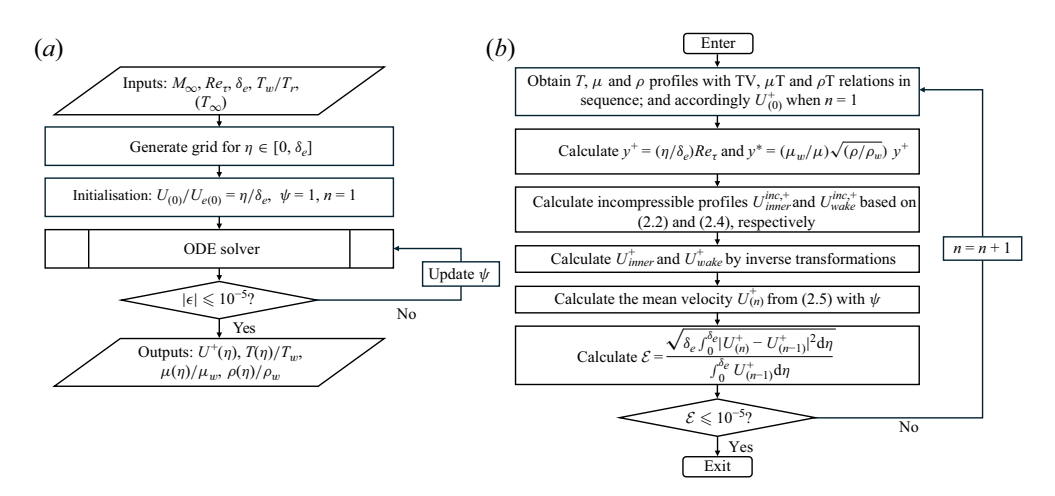


Figure 3. Program chart of the prediction framework: (a) main program, (b) ODE solver.

with the optimal value of sPr equal to 0.8 (Zhang *et al.* 2014). Here, the subscript e denotes the quantities at $y = \delta_e$, and T_r is the recovery temperature. Also, T_e is obtained from the adiabatic wall temperature relation

$$T_r = T_e \left[1 + r \frac{\gamma - 1}{2} M a_e^2 \right], \tag{2.16}$$

with specific heat ratio $\gamma = 1.4$, recovery factor $\gamma = 0.9$ and boundary-layer-edge Mach number $Ma_e = 0.99 \, Ma_{\infty}$.

2.5. Summary of the prediction framework

The prediction framework is summarised in figure 3. The inputs are free-stream Mach number M_{∞} , friction Reynolds number $Re_{\tau} = \delta_e/\delta_v$, δ_e and T_w/T_r , with optionally T_{∞} when the Sutherland's law is applied for the viscosity-temperature (μ T) relation. To numerically solve Π that satisfies the iteration tolerance ($|\epsilon| \le 10^{-5}$), the Newton-Raphson method is applied. The outputs include wall-normal profiles of U^+ , T/T_w , μ/μ_w and ρ/ρ_w . Here, the convergence threshold 10^{-5} is demonstrated to provide converged results, as discussed in Appendix B in detail. The number of iterations required to

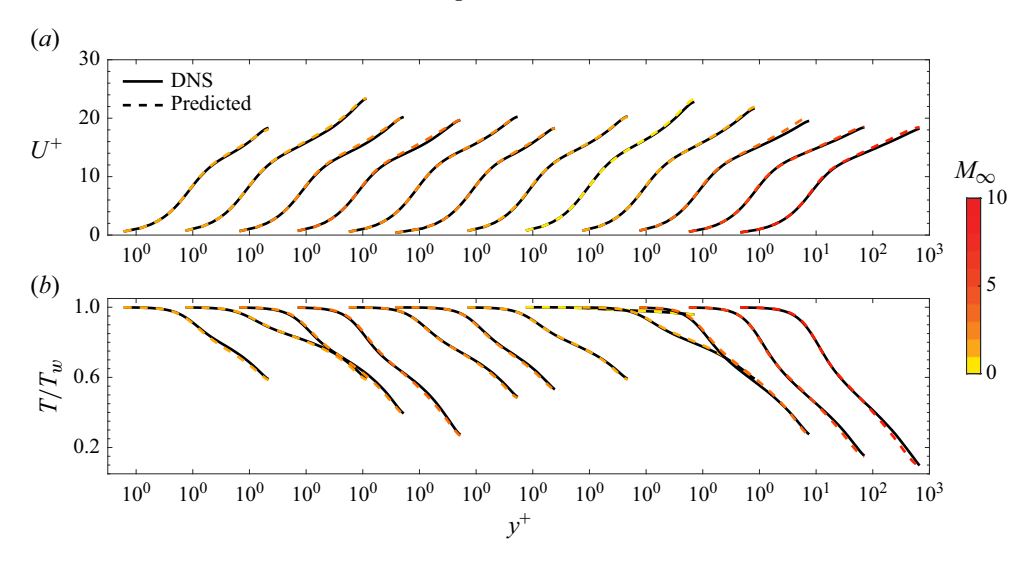


Figure 4. Predicted and DNS results for (a) the mean streamwise velocity, and (b) the temperature, for adiabatic boundary layers. The presented results include, from left to right: $M_{\infty}=2.0$ with $Re_{\tau}=204$, $M_{\infty}=2.0$ with $Re_{\tau}=106$, $M_{\infty}=3.0$ with $Re_{\tau}=502$, $M_{\infty}=4.0$ with $Re_{\tau}=501$ (Pirozzoli & Bernardini 2011); $M_{\infty}=2.5$ with $Re_{\tau}=505$ (Zhang et al. 2018); $M_{\infty}=2.28$ with $Re_{\tau}=224$ (Volpiani et al. 2018); $M_{\infty}=2.0$ with $Re_{\tau}=444$ (Cogo et al. 2022, 2023); $M_{\infty}=0.5$ with $Re_{\tau}=660$, $M_{\infty}=2.0$ with $Re_{\tau}=701$, $M_{\infty}=4.0$ with $Re_{\tau}=709$, $M_{\infty}=6.0$ with $Re_{\tau}=667$, $M_{\infty}=8.0$ with $Re_{\tau}=626$ (Zhang et al. 2022, 2024). The colours (yellow to red) denote M_{∞} (low to high).

reach convergence, and the corresponding computational costs, are also summarised in Appendix B, where the computational robustness and efficiency of the algorithm are demonstrated. Typically, convergence is achieved within 6 iterations and 2.5 s even when the convergence threshold is selected as 10^{-10} , as measured on a desktop computer with an Intel Core i7–8700 CPU @ 3.20 GHz and 32 GB of RAM, running MATLAB in single-threaded mode on Windows 10.

In addition to the algorithm that uses the friction Reynolds number Re_{τ} as input, we also provide an alternative formulation based on the momentum-thickness Reynolds number Re_{θ} , as described in Appendix C, where the results indicate that the error distributions are similar under both input conditions regarding the types of Reynolds numbers.

3. Results

The predicted results for the mean profiles in adiabatic and diabatic TBLs are depicted in figures 4 and 5, respectively. The presented results include the TBLs with lowest and highest values of M_{∞} , Re_{τ} and T_w/T_r , respectively, in each of the six DNS databases. It is found that the predicted mean profiles for velocity and temperature both match well with the DNS results for all the depicted cases. To quantify the overall discrepancy of the velocity profile compared to the actual result, the prediction error $\mathcal{E}(U^+)$ is defined in (2.14), and $\mathcal{E}(T/T_w)$ is defined in the same way but replacing U^+ with T/T_w . As in figure 6(a,b), the prediction errors for mean velocity and temperature are lower than 4.0% and 6.0% in all the tested cases. Here, the higher prediction error in mean temperature should stem from two aspects. First, the wake scaling factor Π is determined according to the self-consistency of the skin-friction coefficient calculated from the velocity profiles. Thus the framework is intrinsically more reliable for the prediction of velocities than that of temperature. Second, when determining the mean temperature profiles from the

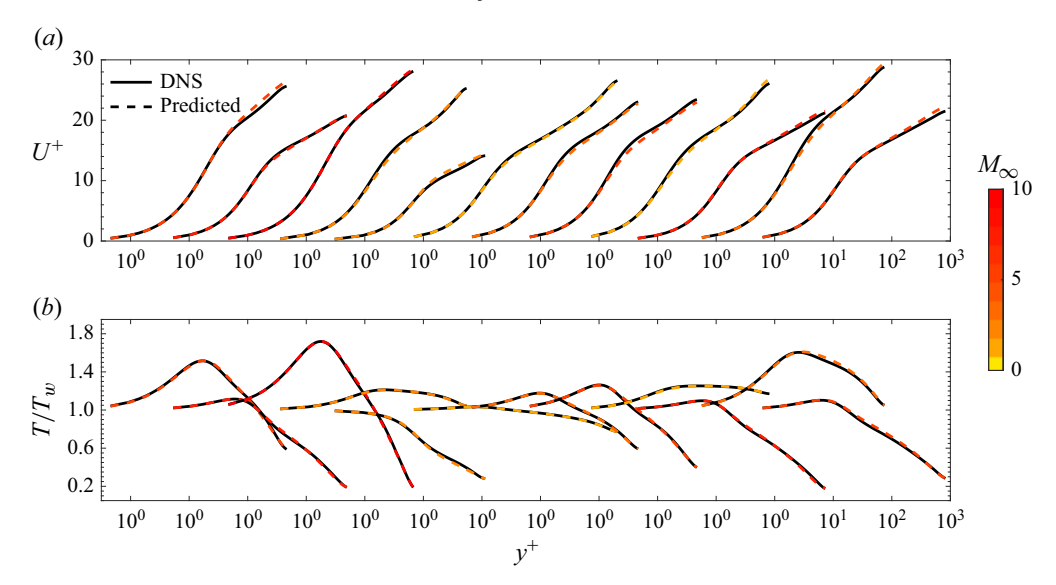


Figure 5. Predicted and DNS results for (a) the mean streamwise velocity, and (b) the temperature, for diabatic boundary layers. The presented results include, from left to right: $M_{\infty} = 5.84$ with $T_w/T_r = 0.25$ and $Re_{\tau} = 436$, $M_{\infty} = 7.87$ with $T_w/T_r = 0.48$ and $Re_{\tau} = 467$, $M_{\infty} = 13.64$ with $T_w/T_r = 0.18$ and $Re_{\tau} = 634$ (Zhang et al. 2018); $M_{\infty} = 2.28$ with $T_w/T_r = 0.5$ and $Re_{\tau} = 512$, $M_{\infty} = 2.28$ with $T_w/T_r = 1.9$ and $Re_{\tau} = 100$ (Volpiani et al. 2018); $M_{\infty} = 2.0$ with $T_w/T_r = 0.76$ and $Re_{\tau} = 1947$, $M_{\infty} = 4.0$ with $T_w/T_r = 0.44$ and $Re_{\tau} = 444$, $M_{\infty} = 6.0$ with $T_w/T_r = 0.35$ and $Re_{\tau} = 444$ (Cogo et al. 2022, 2023); $M_{\infty} = 2.0$ with $T_w/T_r = 0.5$ and $Re_{\tau} = 757$, $M_{\infty} = 8.0$ with $T_w/T_r = 0.5$ and $Re_{\tau} = 683$ (Zhang et al. 2022, 2024); $M_{\infty} = 4.0$ with $T_w/T_r = 0.25$ and $Re_{\tau} = 776$, $M_{\infty} = 6.0$ with $T_w/T_r = 0.5$ and $Re_{\tau} = 779$ (Zhao & Fu 2025).

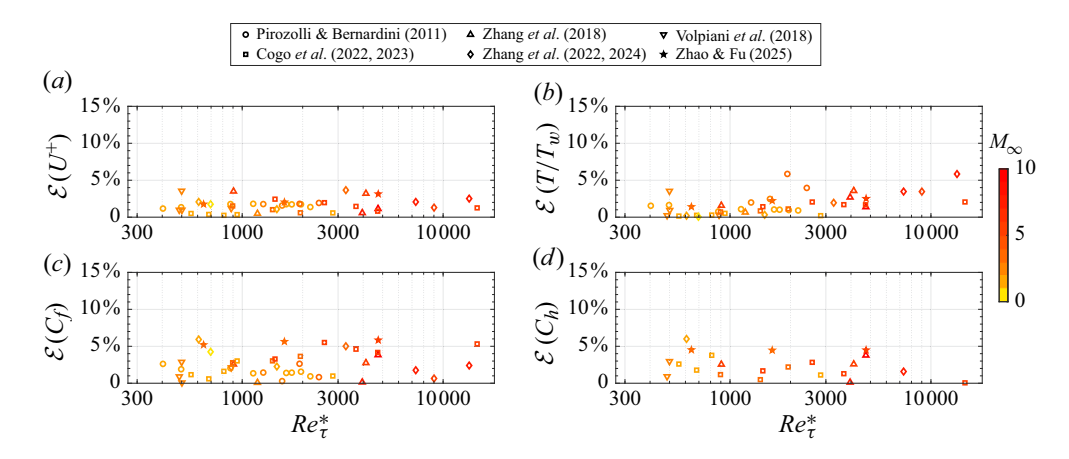


Figure 6. Prediction errors of (a) the mean velocity profile U^+ , (b) the mean temperature profile T/T_w , and (c) the skin-friction coefficient C_f , for all the cases; and (d) wall-heat-transfer coefficient C_h for diabatic cases.

velocity, extra errors are introduced from the TV relation. This highlights the importance of the TV relation for the prediction accuracy of the present framework. In Appendix D, the sources of the prediction errors are further analysed by examining the performance of the underlying scaling laws in the prediction framework under different values of M_{∞} and T_w/T_r . Further, the skin-friction coefficient C_f and wall-heat-transfer coefficient C_h that quantify the wall shear and heat transfer, respectively, are investigated. Here, C_h is defined by $C_h = q_w/(c_p \rho_{\infty} U_{\infty}(T_w - T_r))$, where $q_w = -(c_p/Pr) \mu_w(\partial T/\partial y)_w$, with

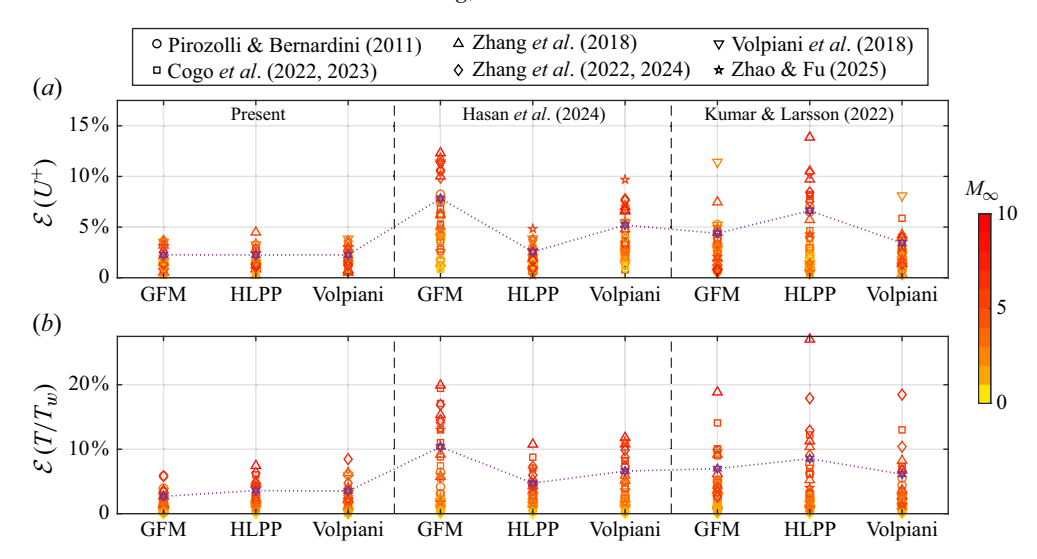


Figure 7. Prediction errors in (a) mean streamwise velocity and (b) temperature. The purple hexagons linked with dotted lines denote the root mean square prediction errors all across the considered TBL cases for each combination of mean-profile-prediction framework and velocity-transformation method.

Pr the Prandtl number, and c_p the isobaric specific heat. The relative errors of C_f and C_h that are defined as $\mathcal{E}(C_f) = \left| (C_{f,P}/C_{f,DNS}) - 1 \right|$ and $\mathcal{E}(C_h) = \left| (C_{h,P}/C_{h,DNS}) - 1 \right|$ are summarised in figure 6(c,d), respectively, where figure 6(d) includes only diabatic cases with non-zero wall heat transfer. It is found that $\mathcal{E}(C_f)$ and $\mathcal{E}(C_h)$ keep relatively low values all across the considered cases, with root mean square values equal to 3.1% and 2.9%, respectively.

Finally, to test the universality of the proposed framework, HLPP (Hasan et al. 2023) and Volpiani (Volpiani et al. 2020), which also perform well in the inner layer, are incorporated into such a framework to replace GFM for inner-layer scaling. The corresponding results for $\mathcal{E}(U^+)$ and $\mathcal{E}(T/T_w)$ are depicted in figure 7. The root mean square prediction errors of all three prediction frameworks incorporating three inner-layer scaling laws are summarised in table 1. Upon applying any of the three considered velocity transformations, the prediction errors of the present framework for mean velocity and temperature are below 5.0 % and 10.0 %, respectively, with average values less than 2.3 % and 3.6 %. For comparison, the GFM, HLPP and Volpiani transformations are further incorporated in the frameworks proposed by Kumar & Larsson (2022) and Hasan et al. (2024). From figure 7, significant increases in the prediction errors are observed in the results from these two frameworks. Since the scaling factors for the wake region in the framework of Hasan et al. (2024) are fitted based on HLPP, this framework performs significantly better when incorporating HLPP than when incorporating GFM or Volpiani. However, even when using HLPP for inner-layer scaling, the prediction errors for mean velocity and temperature profiles with Hasan et al. (2024) are still 13.52 % and 32.42 % higher, respectively, than those obtained with the present framework incorporating HLPP, as indicated by table 1. Hence the validity and universality of the proposed framework are demonstrated.

In addition to the demonstrated validity and universality, it is also worth highlighting another important aspect implied by universality, i.e. future extensibility. The accuracy of the mean profiles predicted by the new framework is fundamentally determined by the four scaling laws mentioned above. As elaborated in Appendix D, the primary sources of

		GFM	HLPP	Volpiani
Present	$U \\ T$	2.26 % 2.69 %	2.25 % 3.58 %	2.25 % 3.51 %
Hasan <i>et al.</i> (2024)	$U \\ T$	7.83 % (+246.00 %) 10.36 % (+284.67 %)	2.55 % (+13.52 %) 4.75 % (+32.42 %)	5.20 % (+130.74 %) 6.60 % (+88.30 %)
Kumar & Larsson (2022)	$U \\ T$	4.38 % (+93.72 %) 6.98 % (+159.27 %)	6.62 % (+194.33 %) 8.53 % (+138.06 %)	3.44 % (+52.52 %) 6.12 % (+74.53 %)

Table 1. Comparisons of the root mean square prediction errors of the newly proposed framework and those proposed by Kumar & Larsson (2022) and Hasan *et al.* (2024). The percentages outside parentheses are the root mean square prediction errors, while those inside parentheses are the increasing ratios of the prediction errors compared to those from the present framework.

the prediction error are attributed to the TV relation and the scaling law for C_f . With the development of more advanced scaling laws in the future, the prediction accuracy of the present framework is expected to be further improved.

4. Concluding remarks

In this study, a universal prediction framework for mean profiles in compressible TBL is proposed, leveraging the established scaling laws regarding velocity transformation, C_f and TV relations. The basic flow properties of Reynolds number, boundary layer thickness, free-stream Mach number and wall-to-recovery ratio are the inputs of such a framework. In the coupled solving procedure for the mean profile, the scalings of flow quantities in the inner layer are reliably described by the velocity transformation (e.g. Volpiani et al. 2020; Griffin et al. 2021b; Hasan et al. 2023), while the mean quantities in the wake region are well determined based on the self-consistency criterion regarding the general scaling law for C_f (Zhao & Fu 2025). The temperature, on the other hand, is obtained from the velocity with the TV relation (Duan & Martín 2011; Zhang et al. 2014). The scaling laws in these three aspects are leveraged in the prediction framework to iteratively refine the mean profiles until the results converge. The prediction framework is applied in compressible TBLs with a fairly wide range of flow conditions, demonstrating 11.9 % to 74.0 % lower root mean square prediction errors in the velocity and temperature profiles compared to existing mean-profile-prediction frameworks. Especially for all three velocity transformation methods used for inner-layer scaling, the root mean square prediction errors in the mean velocity and temperature profiles remain below 2.3 % and 3.6 %, respectively. Such robust validity of the present framework with different velocity transformations highlights its universality among the established and future scaling laws.

The four scaling laws underlying the proposed framework – i.e. inner-layer scaling, outer-layer scaling, the general scaling law for skin-friction coefficient and TV relation – are well established only for canonical equilibrium wall-bounded turbulence in the current stage. Moreover, as comprehensively tested in Bai, Griffin & Fu (2022), the existing velocity transformations do not deliver satisfying performance for non-canonical TBLs under high-enthalpy or supercritical conditions. Such facts indicate that the framework incorporating the currently established scaling laws is applicable only to canonical zero-pressure-gradient TBLs. On the other hand, the application of the framework in non-equilibrium flows would require the future development the scaling laws that are valid under the non-canonical conditions. It should be noted that our proposed framework is built upon the universal self-consistency criterion regarding the skin-friction coefficient

rather than tied to any specific scaling, which is thus inherently general. Therefore, with appropriate scaling laws for non-canonical TBLs developed in the future, the proposed framework is expected to be naturally extended to such cases.

The proposed prediction framework is of importance in fundamental research and engineering applications. For high-speed or high-Reynolds-number flows whose mean properties are expensive to obtain from experiments or DNS, the proposed prediction framework provides reliable predictions of their mean properties that are essential for evaluating the skin friction and heat transfer. Besides, the predicted mean profiles can also be applied for initialisation of the flow field and providing inflow conditions for the numerical simulations of a compressible TBL, which is expected to shorten the recovery distance and thus reduce the computational cost.

Acknowledgements. We thank the anonymous reviewers for their valuable comments and suggestions.

Funding. L.F. acknowledges the fund from the National Natural Science Foundation of China (no. 12422210), the Research Grants Council (RGC) of the Government of Hong Kong Special Administrative Region (HKSAR) with RGC/ECS Project (no. 26200222), RGC/GRF Project (no. 16201023), RGC/STG Project (no. STG2/E-605/23-N) and RGC/TRS Project (no. T22-607/24N), and the fund from Guangdong Basic and Applied Basic Research Foundation (no. 2024A1515011798).

Data availability statement. The data that support the findings of this study are available on request from the corresponding author, L.F.

Declaration of interests. The authors report no conflict of interest.

Appendix A. Inverse GFM transformation

The forward GFM transformation (Griffin et al. 2021b) is expressed as

$$\frac{\mathrm{d}U^{inc,+}}{\mathrm{d}y^*} = \frac{\frac{1}{\mu^+} \frac{\mathrm{d}U^+}{\mathrm{d}y^*}}{1 + \frac{1}{\mu^+} \frac{\mathrm{d}U^+}{\mathrm{d}y^*} - \mu^+ \frac{\mathrm{d}U^+}{\mathrm{d}y^+}},\tag{A1}$$

which can be rearranged to

$$\frac{1}{\mu^{+}} \frac{dU^{+}}{dy^{*}} = \left(1 + \frac{1}{\mu^{+}} \frac{dU^{+}}{dy^{*}} - \mu^{+} \frac{dU^{+}}{dy^{+}}\right) \frac{dU^{inc,+}}{dy^{*}}
= \frac{dU^{inc,+}}{dy^{*}} + \frac{1}{\mu^{+}} \frac{dU^{+}}{dy^{*}} \frac{dU^{inc,+}}{dy^{*}} - \mu^{+} \frac{dU^{+}}{dy^{+}} \frac{dU^{inc,+}}{dy^{*}}.$$
(A2)

According to the chain rule, (A2) is further derived to be

$$\begin{split} \frac{1}{\mu^{+}} \frac{\mathrm{d}U^{+}}{\mathrm{d}y^{*}} &= \frac{\mathrm{d}U^{inc,+}}{\mathrm{d}y^{*}} + \frac{1}{\mu^{+}} \frac{\mathrm{d}U^{+}}{\mathrm{d}y^{*}} \frac{\mathrm{d}U^{inc,+}}{\mathrm{d}y^{*}} - \mu^{+} \frac{\mathrm{d}U^{+}}{\mathrm{d}y^{+}} \left(\frac{\mathrm{d}y^{+}}{\mathrm{d}y^{*}} \frac{\mathrm{d}y^{*}}{\mathrm{d}y^{+}} \right) \frac{\mathrm{d}U^{inc,+}}{\mathrm{d}y^{*}} \\ &= \frac{\mathrm{d}U^{inc,+}}{\mathrm{d}y^{*}} + \frac{1}{\mu^{+}} \frac{\mathrm{d}U^{+}}{\mathrm{d}y^{*}} \frac{\mathrm{d}U^{inc,+}}{\mathrm{d}y^{*}} - \mu^{+} \frac{\mathrm{d}U^{+}}{\mathrm{d}y^{*}} \frac{\mathrm{d}U^{inc,+}}{\mathrm{d}y^{+}}. \end{split} \tag{A3}$$

Equation (A3) is further rearranged to

$$\frac{1}{\mu^{+}} \frac{dU^{+}}{dy^{*}} - \frac{1}{\mu^{+}} \frac{dU^{+}}{dy^{*}} \frac{dU^{inc,+}}{dy^{*}} + \mu^{+} \frac{dU^{+}}{dy^{*}} \frac{dU^{inc,+}}{dy^{+}} = \frac{dU^{inc,+}}{dy^{*}}$$

$$\Rightarrow \frac{dU^{+}}{dy^{*}} \left(\frac{1}{\mu^{+}} - \frac{1}{\mu^{+}} \frac{dU^{inc,+}}{dy^{*}} + \mu^{+} \frac{dU^{inc,+}}{dy^{+}} \right) = \frac{dU^{inc,+}}{dy^{*}}$$

$$\Rightarrow \frac{dU^{+}}{dy^{*}} = \frac{\frac{dU^{inc,+}}{dy^{*}}}{\frac{1}{\mu^{+}} - \frac{1}{\mu^{+}} \frac{dU^{inc,+}}{dy^{*}} + \mu^{+} \frac{dU^{inc,+}}{dy^{+}}}.$$
(A4)

The inverse GFM transformation is thereby obtained in (A4), by which the incompressible velocity profile is transformed to its compressible counterpart with given temperature and viscosity profiles.

Appendix B. Flow parameters and convergence test of the framework

The flow parameters of the 44 cases of compressible TBLs from six DNS databases (Pirozzoli & Bernardini 2011; Zhang *et al.* 2018, 2022, 2024; Volpiani *et al.* 2018; Cogo *et al.* 2022, 2023; Zhao & Fu 2025) are summarised in table 2, including information for free-stream Mach number Ma_{∞} (0.5–13.64), wall-to-recovery ratio T_w/T_r (0.25–1.9), friction Reynolds number Re_{τ} (100–1947), boundary-layer-thickness-based Reynolds number Re_{δ_e} (10 216–1 343 863) and momentum-thickness-based Reynolds number Re_{θ} (877–41 172).

Meanwhile, the number of iterations and execution time required for our proposed framework, incorporating GFM for inner-layer scaling, to reach the convergence thresholds 10^{-5} and 10^{-10} are also summarised in table 2. Here, the numbers of iterations refer to those of the outer loop sketched in figure 3(a), which updates the wake scaling factor Π at each step. In all the cases, the number of iterations is no more than 5 and 6 for convergence thresholds 10^{-5} and 10^{-10} , respectively, which indicates that the values of Π quickly converge during the iterations, and thus demonstrates the robustness of the algorithm. On the other hand, the total execution time is less than 2.5 seconds, with each iteration taking less than 0.4 seconds, as measured on a desktop computer with an Intel Core i7–8700 CPU @ 3.20 GHz and 32 GB of RAM, running MATLAB in single-threaded mode on Windows 10. Such computational costs are negligible compared to those of the DNS, which demonstrates the robustness and efficiency of the present framework.

To further test the impact of the convergence threshold on the prediction results, those with 10^{-10} for both the outer loop and the ODE solver are compared with those with 10^{-5} as adopted in the main text. To quantify their difference, $\mathcal{D}(U^+)$ is defined here with

$$\mathcal{D}(U^{+}) = \sqrt{\frac{1}{\delta_{e}} \int_{0}^{\delta_{e}} \left(U_{(10^{-10})}^{+}(\eta) - U_{(10^{-5})}^{+}(\eta) \right)^{2} d\eta} / \left(\frac{1}{\delta_{e}} \int_{0}^{\delta_{e}} U_{(10^{-10})}^{+}(\eta) d\eta \right), \quad (B1)$$

where $U_{(10^{-5})}^+$ and $U_{(10^{-10})}^+$ are the predictions with thresholds 10^{-5} and 10^{-10} , respectively. We define $\mathcal{D}(T/T_w)$ in the same way as $\mathcal{D}(U^+)$ by replacing U^+ with T/T_w in (B1). The values of $\mathcal{D}(U^+)$ for all the tested cases are summarised in figure 8. For all the cases, the differences in the predicted results with different convergence thresholds are lower than 10^{-5} , i.e. 0.001~%, which is negligible for the results. Thus the threshold 10^{-5} is considered to yield converged results.

Reference	Ma	T /T	D _o	D _o	D _o	Number of	Execution
Reference	Ma_{∞}	T_w/T_r	Re_{τ}	Re_{δ_e}	Re_{θ}	iterations	time (s)
Pirozzoli & Bernardini (2011)	2.0	1.0	204	10 216	877	4 (5)	0.4040 (0.6746)
	2.0	1.0	251	13 012	1131	4(5)	0.3933 (0.5937)
	2.0	1.0	445	24 792	2090	3 (5)	0.3838 (0.6538)
	2.0	1.0	580	33 702	2890	4 (5)	0.4754 (0.6849)
	2.0	1.0	838	51 312	4437	4 (5)	0.6417 (0.9278)
	2.0	1.0	893	55 170	4760	4 (5)	0.6813 (0.9061)
	2.0	1.0	992	62 125	5347	3 (5)	0.5378 (0.8822)
	2.0	1.0	1106	70 513	6045	3 (5)	0.5435 (0.9103)
	3.0	1.0	403	44 654	3013	4 (5)	0.4715 (0.7186)
	3.0	1.0	502	57 893	3955	4 (5)	0.5107 (0.7672)
	4.0	1.0	395	83 623	4713	4 (5)	0.5308 (0.8153)
	4.0	1.0	501	107 715	5943	4 (5)	0.5261 (0.8345)
Zhang et al. (2018)	2.50	1.0	510	36 944	2835	4 (4)	0.7286 (0.8225)
	5.84	0.25	450	37 385	2121	5 (6)	1.1732 (1.2064)
	5.86	0.76	453	242 029	9455	5 (6)	1.0748 (1.1391)
	7.87	0.48	480	287 338	9714	5 (6)	1.1841 (1.2883)
	13.64	0.18	646	701 454	14 408	5 (6)	1.9773 (2.2372)
Volpiani et al. (2018)	2.28	0.5	512	11 997	1251	3 (5)	0.5665 (1.0361)
	2.28	1.0	395	24 328	1989	4 (5)	0.6641 (0.9320)
	2.28	1.0	224	12 628	1047	4 (5)	0.5539 (0.7967)
	2.28	1.9	100	13 440	868	4 (6)	0.5160 (0.9741)
Cogo et al. (2023)	2.0	0.76	1947	87 859	7954	4 (4)	1.2768 (1.4397)
	2.0	0.69	444	13 399	1242	4 (5)	0.5288 (0.7561)
	2.0	0.79	443	16 609	1486	4 (5)	0.5260 (0.7299)
	2.0	0.90	443	19 971	1714	4 (5)	0.5357 (0.7433)
	2.0	1.0	444	23 633	1981	4 (4)	0.5261 (0.6423)
	4.0	0.44	444	27 001	1848	4 (5)	0.5780 (0.9278)
	4.0	0.63	444	44 215	2749	4 (5)	0.5692 (0.8372)
	4.0	0.81	444	63 551	3657	4 (5)	0.6367 (0.8536)
	5.86	0.76	1947	996 276	41 172	4 (5)	0.1248 (1.7653)
	6.0	0.35	444	56 610	2813	4 (5)	0.6430 (0.9729)
	6.0	0.57	444	108 382	4841	5 (6)	0.7596 (1.1140)
	6.0	0.78	444	166 073	6643	5 (6)	0.8024 (1.1388)
	6.0	1.0	444	228 481	8401	5 (6)	0.7873 (1.1601)
Zhang et al. (2022, 2024)	0.5	1.0	660	16 335	1847	3 (5)	0.5619 (0.7109)
	2.0	1.0	771	43 744	3790	4 (5)	0.7328 (0.9290)
	2.0	0.5	757	14 865	1591	3 (5)	0.5727 (0.7762)
	4.0	1.0	709	139 990	7653	4 (6)	0.8959 (0.1389)
	6.0	1.0	667	592 097	21 797	5 (6)	1.0296 (1.3740)
	8.0	1.0	626	1 343 863	35 628	5 (6)	1.1503 (1.8410)
	8.0	0.5	683	524 923	17 858	5 (6)	1.1314 (1.4859)
Zhao & Fu (2025)	4.0	0.5	751	55 803	3716	4 (5)	0.8247 (0.9566)
	4.0	0.25	706	19 231	1534	4 (5)	0.8241 (0.9387)
	6.0	0.5	779	235 936	10630	5 (6)	1.1367 (1.2571)

Table 2. Summary of flow parameters for the compressible TBLs in fully developed turbulent regions used in this study. The rightmost two columns show the number of iterations and execution times required for our framework with GFM-based inner-layer transformation to reach the convergence thresholds. Values outside parentheses correspond to convergence thresholds 10^{-5} for both the outer loop and ODE solver; values inside parentheses correspond to thresholds 10^{-10} .

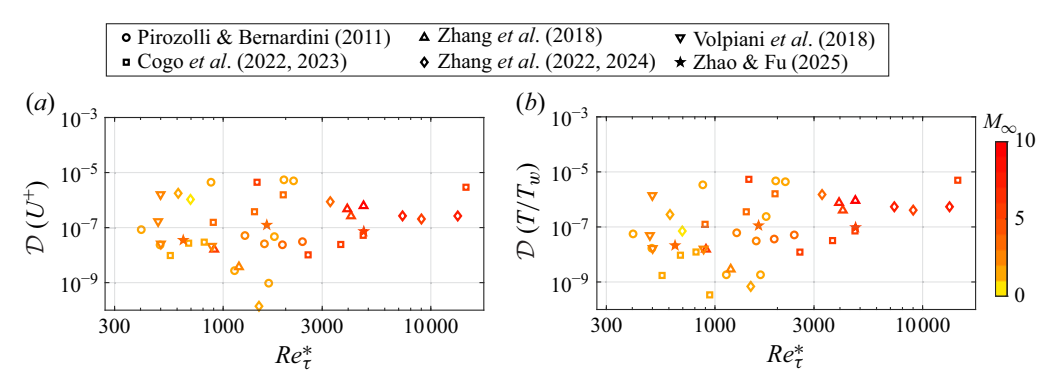


Figure 8. Differences of the prediction results with convergence thresholds 10^{-5} and 10^{-10} for (a) mean streamwise velocity and (b) mean temperature.

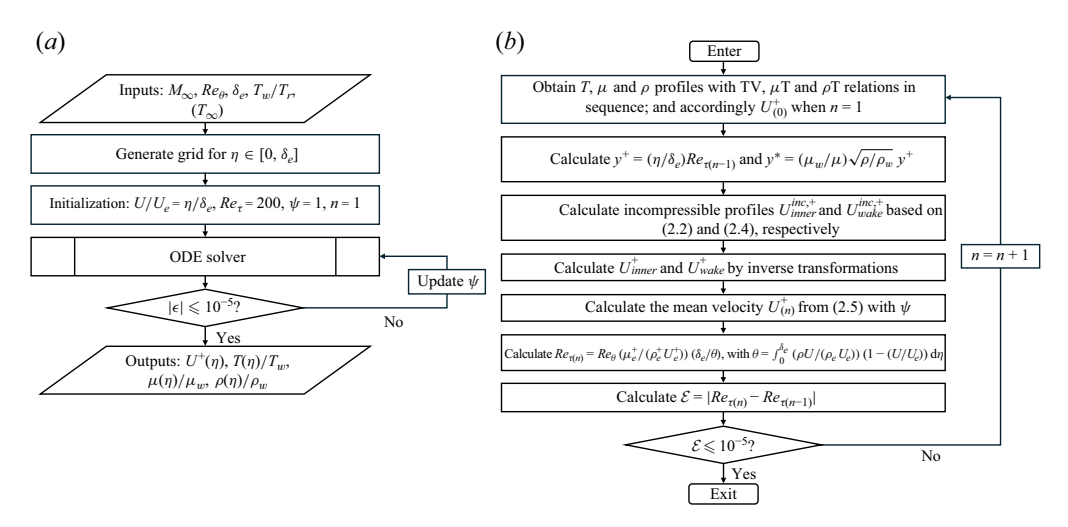


Figure 9. Program chart of the prediction framework with Re_{θ} as input: (a) main program, (b) ODE solver.

Appendix C. Prediction framework with the momentum-thickness-based Reynolds number as input

In the main text, the friction Reynolds number Re_{τ} is utilised as an input of the prediction framework, which is summarised in figure 3. In this appendix, the alternative algorithm based on the momentum-thickness-based Reynolds number Re_{θ} is presented, as in figure 9. Such an algorithm differs slightly from that with Re_{τ} as input. Here, the unknown Re_{τ} is updated at each step in the ODE solver until the results converge, while the core idea of the proposed framework, i.e. self-consistency regarding the skin-friction coefficient, is retained. Comparisons between the prediction results with Re_{τ} and Re_{θ} as inputs are depicted in figure 10. Although minor differences exist, the results show that the error distributions are similar under both input conditions. The consistency between the results with Re_{θ} and Re_{τ} as inputs further demonstrates the universality of the proposed framework.

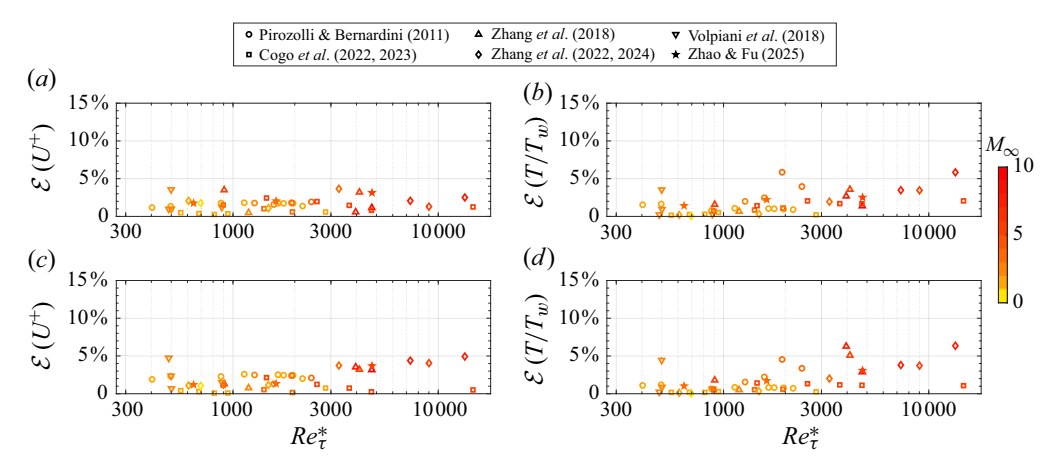


Figure 10. Prediction errors of (a,c) the mean velocity profile U^+ and (b,d) the mean temperature profile T/T_w that are obtained from inputs (a,b) Re_{τ} and (c,d) Re_{θ} .

Appendix D. Discussions on the sources of prediction error

The prediction error in our framework comes from the four underlying scaling laws, i.e. the inner-layer velocity scaling, the outer-layer velocity scaling, the TV relation and the general scaling law for the skin-friction coefficient (C_f). In Griffin *et al.* (2021b), it is demonstrated that the GFM transformation performs well for inner-layer velocity scaling with a wide range of flow conditions for canonical wall-bounded turbulence. Thus it is not considered to be the main source of prediction error in the canonical TBL cases tested in this study. On the other hand, while the outer-layer scaling shapes the wake region, its magnitude is determined by the scaling law for C_f . Thus the main sources of error are considered to be the TV relation and the scaling law for C_f . To clarify the contributions of each to the overall prediction error, we perform *a priori* analyses for each of these two types of scaling laws.

To quantify the prediction error of the TV relation (Duan & Martín 2011; Zhang *et al.* 2012), the predicted mean temperature profiles $T^+ = T/T_w$ based on the actual mean velocity profiles from DNS with

$$\frac{T}{T_e} = \frac{T_w}{T_e} + \frac{T_r - T_w}{T_e} \left[(1 - sPr) \left(\frac{U}{U_e} \right)^2 + sPr \left(\frac{U}{U_e} \right) \right] + \frac{T_e - T_r}{T_e} \left(\frac{U}{U_e} \right)^2$$
(D1)

are compared with the mean temperature directly from the DNS, where the prediction error $\mathcal{E}(T/T_w)$ is defined in the same way as in (2.14), identical to that used in the main text. To investigate the impacts of M_∞ and T_r/T_w on the performance of the established TV relation, the values of $\mathcal{E}(T/T_w)$ are depicted in figures 11(a) and 12(a) versus Re_τ^* , where the symbols are coloured based on M_∞ and T_r/T_w , respectively. It is found that the prediction error of T/T_w notably increases as Re_τ^* increases. On the other hand, the increases of M_∞ and T/T_w also appear to enlarge the prediction error, although the sole increase of each one of them does not show a unified effect. Considering that the increases of M_∞ or T/T_w at given T/T_w or M_∞ both enlarge the value of Re_τ^* , we conclude that the performance of the current TV relation is negatively affected by both free-stream Mach number and wall heat transfer.

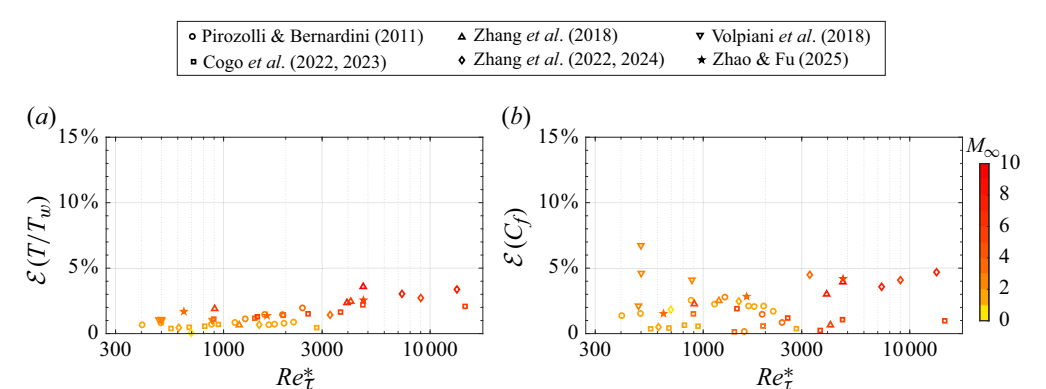


Figure 11. Prediction errors of (a) the TV relation (Duan & Martín 2011; Zhang et al. 2012) for mean temperature profile and (b) the general scaling law (Zhao & Fu 2025) for the skin-friction coefficient. The colours of the scattered symbols (yellow to red) denote the free-stream Mach number.

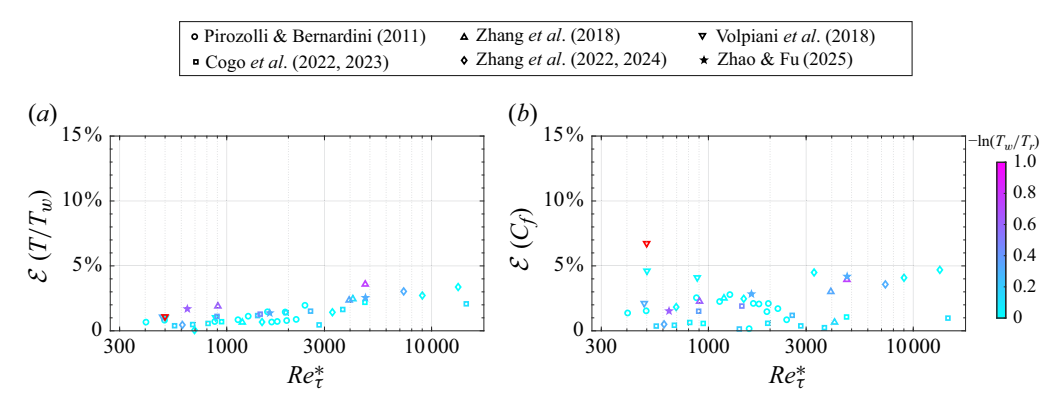


Figure 12. Prediction errors of (a) the TV relation (Duan & Martín 2011; Zhang et al. 2012) for mean temperature profile and (b) the general scaling law (Zhao & Fu 2025) for the skin-friction coefficient. The colours of the scattered symbols (cyan to magenta) denote $-\ln(T_w/T_r)$. The only symbol coloured with red denotes the hot-wall case from Volpiani et al. (2018) with $M_\infty = 2.28$ and $T_w/T_r = 1.9$.

To analyse the performance of the general scaling law for C_f (Zhao & Fu 2025) as defined in (2.8), the prediction error $\mathcal{E}(C_f)$ is defined by

$$\mathcal{E}(C_f) = \left| \left(\frac{2}{C_{f,i}} \right)^{1/2} - \left(\frac{1}{\kappa_f} \ln Re_{\theta,i} + C \right) \right| / \left(\frac{2}{C_{f,i}} \right)^{1/2}. \tag{D2}$$

The values of $\mathcal{E}(C_f)$ are shown in figures 11(b) and 12(b) as functions of Re_{τ}^* . As with the mean temperature results, the data points are colour-coded according to M_{∞} and T_w/T_r , respectively, to examine the effects of these parameters. In contrast to the TV relation, the scaling law for C_f does not display a significant dependence on either M_{∞} or T_w/T_r . For example, cases from Volpiani *et al.* (2018) with $M_{\infty} = 2.28$ exhibit prediction errors similar to those for $M_{\infty} = 8.0$ from Zhang *et al.* (2024) – both approximately 5%. These results indicate that the performance of the established scaling law for C_f is not substantially affected by the free-stream Mach number or wall heat transfer, while the prediction results scatter within range approximately 5% relative to the DNS results.

According to the above discussions, the sources of prediction error are identified into two aspects. First, the increases of M_{∞} , T_w/T_r and Re_{τ}^* enlarge the prediction errors of

the TV relation. Second, the prediction errors from the scaling law of C_f are not notably affected by M_{∞} and T_w/T_r , but distribute from 0 to approximately 5 %. The improvement of the accuracy of the prediction framework relies on the further advancements of the TV relation and the scaling law of C_f , which are anticipated to be developed in future work.

REFERENCES

- BAI, T., GRIFFIN, K.P. & FU, L. 2022 Compressible velocity transformations for various noncanonical wall-bounded turbulent flows. *AIAA J.* **60** (7), 4325–4337.
- BRADSHAW, P. 1977 Compressible turbulent shear layers. Annu. Rev. Fluid Mech. 9, 33–52.
- CHEN, X., GAN, J. & Fu, L. 2024 An improved Baldwin–Lomax algebraic wall model for high-speed canonical turbulent boundary layers using established scalings. *J. Fluid Mech.* **987**, A7.
- COGO, M., BAÙ, U., CHINAPPI, M., BERNARDINI, M. & PICANO, F. 2023 Assessment of heat transfer and Mach number effects on high-speed turbulent boundary layers. *J. Fluid Mech.* **974**, A10.
- COGO, M., SALVADORE, F., PICANO, F. & BERNARDINI, M. 2022 Direct numerical simulation of supersonic and hypersonic turbulent boundary layers at moderate-high Reynolds numbers and isothermal wall condition. J. Fluid Mech. 945, A30.
- COLES, D. 1956 The law of the wake in the turbulent boundary layer. J. Fluid Mech. 1 (2), 191–226.
- VAN DRIEST, E.R. 1951 Turbulent boundary layer in compressible fluids. J. Astronaut. Sci. 18 (3), 145–160.
- VAN DRIEST, E.R. 1956 The problem of aerodynamic heating. Aeronaut. Engng Rev. 15 (10), 26-41.
- DUAN, L., BEEKMAN, I. & MARTÍN, M.P. 2010 Direct numerical simulation of hypersonic turbulent boundary layers. Part 2. Effect of wall temperature. J. Fluid Mech. 655, 419–445.
- DUAN, L., BEEKMAN, I. & MARTÍN, M.P. 2011 Direct numerical simulation of hypersonic turbulent boundary layers. Part 3. Effect of Mach number. *J. Fluid Mech.* **672**, 245–267.
- DUAN, L. & MARTÍN, M.P. 2011 Direct numerical simulation of hypersonic turbulent boundary layers. Part 4. Effect of high enthalpy. J. Fluid Mech. 684, 25–59.
- GRIFFIN, K.P., FU, L. & MOIN, P. 2021a The effect of compressibility on grid-point and time-step requirements for simulations of wall-bounded turbulent flows. In *Center for Turbulence Research Annual Research Briefs* (ed. P. Moin), pp. 109–117. Center for Turbulence Research.
- GRIFFIN, K.P., Fu, L. & Moin, P. 2021b Velocity transformation for compressible wall-bounded turbulent flows with and without heat transfer. *Proc. Natl Acad. Sci.* 118 (34), e2111144118.
- GRIFFIN, K.P., Fu, L. & Moin, P. 2023 Near-wall model for compressible turbulent boundary layers based on an inverse velocity transformation. *J. Fluid Mech.* **970**, A36.
- HASAN, A.M., LARSSON, J., PIROZZOLI, S. & PECNIK, R. 2023 Incorporating intrinsic compressibility effects in velocity transformations for wall-bounded turbulent flows. *Phys. Rev. Fluids* 8 (11), L112601.
- HASAN, A.M., LARSSON, J., PIROZZOLI, S. & PECNIK, R. 2024 Estimating mean profiles and fluxes in high-speed turbulent boundary layers using inner/outer-layer scalings. *AIAA J.* **62** (2), 848–853.
- HUANG, P.G., BRADSHAW, P. & COAKLEY, T.J. 1993 Skin friction and velocity profile family for compressible turbulent boundary layers. AIAA J. 31 (9), 1600–1604.
- JOHNSON, D.A. & KING, L.S. 1985 A mathematically simple turbulence closure model for attached and separated turbulent boundary layers. AIAA J. 23 (11), 1684–1692.
- KAWAI, S. & LARSSON, J. 2012 Wall-modeling in large eddy simulation: length scales, grid resolution, and accuracy. *Phys. Fluids* 24 (1), 015105.
- KUMAR, V. & LARSSON, J. 2022 Modular method for estimation of velocity and temperature profiles in high-speed boundary layers. *AIAA J.* **60** (9), 5165–5172.
- MORKOVIN, M.V. 1962 Effects of compressibility on turbulent flows. Mécanique Turbul. 367 (380), 26.
- PIROZZOLI, S. & BERNARDINI, M. 2011 Turbulence in supersonic boundary layers at moderate Reynolds number. J. Fluid Mech. 688, 120–168.
- SPALDING, D.B. & CHI, S.W. 1964 The drag of a compressible turbulent boundary layer on a smooth flat plate with and without heat transfer. *J. Fluid Mech.* **18** (1), 117–143.
- Trettel, A. & Larsson, J. 2016 Mean velocity scaling for compressible wall turbulence with heat transfer. *Phys. Fluids* **28** (2), 026102.
- VOLPIANI, P.S., BERNARDINI, M. & LARSSON, J. 2018 Effects of a nonadiabatic wall on supersonic shock/boundary-layer interactions. *Phys. Rev. Fluids* 3 (8), 083401.
- VOLPIANI, P.S., IYER, P.S., PIROZZOLI, S. & LARSSON, J. 2020 Data-driven compressibility transformation for turbulent wall layers. *Phys. Rev. Fluids* 5 (5), 052602.
- ZHANG, C., DUAN, L. & CHOUDHARI, M.M. 2018 Direct numerical simulation database for supersonic and hypersonic turbulent boundary layers. *AIAA J.* 56 (11), 4297–4311.

- ZHANG, P.-J.-Y., WAN, Z.-H., LIU, N.-S., SUN, D.-J. & LU, X.-Y. 2022 Wall-cooling effects on pressure fluctuations in compressible turbulent boundary layers from subsonic to hypersonic regimes. *J. Fluid Mech.* **946**, A14.
- ZHANG, P.-J.-Y., WAN, Z.-H., SUN, D.-J. & LU, X.-Y. 2024 The intrinsic scaling relation between pressure fluctuations and Mach number in compressible turbulent boundary layers. *J. Fluid Mech.* 993, A2.
- ZHANG, Y.-S., BI, W.-T., HUSSAIN, F., LI, X.-L. & SHE, Z.-S. 2012 Mach-number-invariant mean-velocity profile of compressible turbulent boundary layers. *Phys. Rev. Lett.* **109** (5), 054502.
- ZHANG, Y.-S., BI, W.-T., HUSSAIN, F. & SHE, Z.-S. 2014 A generalized Reynolds analogy for compressible wall-bounded turbulent flows. *J. Fluid Mech.* **739**, 392–420.
- ZHAO, Z. & FU, L. 2025 Revisiting the theory of van Driest: a general scaling law for the skin-friction coefficient of high-speed turbulent boundary layers. *J. Fluid Mech.* **1012**, R3.